Spatial-temporal dynamics of a microbial cooperative behavior robust to cheating

Hilary Monaco[1, 2], Tiago Sereno[2], Kevin Liu[3], Caleb Reagor[1], Maxime Deforet[4], Joao B. Xavier[2*]

[1]Weill Cornell Medicine, Tri-Institutional PhD Program in Computational Biology and Medicine, New York, NY, USA

[2]Program for Computational and Systems Biology, Memorial Sloan-Kettering Cancer Center, New York, NY, USA

[3]Summer Undergraduate Research Program, Memorial Sloan-Kettering Cancer Center, New York, NY USA

[4]Sorbonne Université, CNRS, Institut de Biologie Paris-Seine (IBPS), Laboratoire Jean Perrin (LJP), F-75005, Paris, France

*Corresponding Author at xavierj@mskcc.org

Abstract

Individuals living in dense populations control their behaviors by sensing, integrating and responding to many cues. How can these processes enable the evolution and stability of cooperative behaviors that could easily be exploited by cheaters? Here we shed light on how bacteria regulate cooperation by studying swarming in *Pseudomonas aeruginosa*, a behavior requiring cooperative secretions of rhamnolipid surfactants to facilitate collective movement over surfaces. By combining fluorescent imaging and computational analyses we show, counterintuitively, that rhamnolipid expression peaks at swarming edges. We then show that the integration of competing diffusive cues—quorum sensing signals and growth-limiting nutrients—enables *P. aeruginosa* to communicate across centimeters and adopt expression patterns unseen in well-mixed liquid culture. Integration of multiple cues enables robustness against cheating even when we experimentally perturb the quorum sensing system. Taken together, these results illuminate how the integration of cues in spatially structured communities can stabilize cooperation.

Introduction

Cooperation between cells allows microbes to contribute to multicellular communities ranging from antibiotic resistant biofilms (Costerton et al. 1999; Lee et al. 2010), fruiting bodies (Velicer and Vos 2009), swarming motility (Yan et al. 2019) and impact macroscopic organisms in ways that no individual microbe alone could (Singh et al. 2000; Rutherford and Bassler 2012). However, the microenvironments experienced by individual microbes living inside a densely microbial community are dynamic, densely packed and competitive (Granato et al. 2019). Cooperative traits can come at a cost to individuals because they require resources that could otherwise be used to grow (Griffin et al. 2004). How can microbial cooperative traits evolve and remain stable in nature in the competitive environment of bacterial communities? Understanding the cell-level computation that leads to evolutionary robustness of cooperative behaviors remains an open problem in sociomicrobiology. Spatial structure is key to the evolution of cooperation. Even a costly cooperative trait can be preserved as long as the benefits of cooperating can be localized to regions of highly related individuals (Nadell et al. 2010; Nadell et al. 2013; Kim et al. 2014; Drescher et al. 2014).

Microbes have the ability to sense, integrate and respond to diffusible queues by changing their gene expression. The concentrations of diffusible molecules that cells consume (such as nutrients) or produce (such as quorum sensing signals) change in time and with the dynamics of the rest of the surrounding cellular community. The spatial distribution of growth-limiting resources influences the development of structured populations, even in macroscopic communities: Vegetation growing in arid landscapes where water is the most limiting resource often show spatially structured patterning (Lejeune et al. 2004; Rietkerk et al. 2002; Rietkerk et al. 2004). The interactions between plants in arid environments can be described using an

52 ecological kernel, where positive interactions represent nutrient preservation and negative ones,
53 nutrient competition. Ecological kernels can also provide insights into the spatial structure of
54 microbial communities (Deng et al. 2014), by describing how competing diffusible signals—
55 growth limiting nutrients and quorum sensing signals—can influence the expression of a
56 cooperative gene.

57 Here we investigate how the environment experienced by microbes influences their
58 dynamics of cooperative behavior in spatially structured environments. We focus on the gram-
59 negative *Pseudomonas aeruginosa*, an opportunistic pathogen often used as a model to study
60 bacterial social behavior. *P. aeruginosa* builds thick antibiotic resistant biofilms that are life-
61 threatening lung infections to cystic fibrosis patients and secrete a swath of disease-inducing
62 virulence factors (Rutherford and Bassler 2012). These bacteria communicate by quorum sensing
63 and transition between sessile (biofilm) and motile (swarming) life styles (Yan et al. 2019). *P.*
64 *aeruginosa* swarms are of particular interest for their evolutionary robustness. This cooperative
65 behavior allows a colony to grow over an order of magnitude larger in final population size
66 (Xavier et al. 2011) but requires the expression of *rhlA* (Zhu and Rock 2008; Caiazza et al. 2005)
67 and the subsequent secretion of massive amounts of rhamnolipid biosurfactant molecules
68 (Caiazza et al. 2005; Déziel et al. 2003) that can amount to 20% of their dry mass (Xavier et al.
69 2011).

70 Secreted molecules required for swarming become publicly available once released, but
71 the cooperative behavior remains robust to cheating. Wild type *P. aeruginosa* does not lose in
72 competition against a Δ*rhlA* mutant unable to produce rhamnolipids thanks to the dynamic
73 regulation of *rhlA* which integrates of quorum signals and information nutrient availability to
74 delay expression to times when rhamnolipid secretion becomes affordable (Xavier et al. 2011; de

75 Vargas Roditi et al. 2013; Boyle et al. 2015). The ability to regulate investment in a cooperative
76 trait to avoid a fitness cost is termed Metabolic Prudence (Xavier et al. 2011), a strategy that may
77 regulate many bacterial social traits (Xavier et al. 2011; Mellbye and Schuster 2014; Smith and
78 Schuster 2019).

79 Rhamnolipids are a high carbon-content compound. Experiments tracking gene
80 expression in liquid culture showed that if cells run out of carbon source, they shut off *rhlA*
81 expression. When cells run out of either nitrogen or iron instead, cells ramp up *rhlA* expression
82 and allocate carbon towards rhamnolipid synthesis. This is presumably to facilitate movement to
83 more nutrient rich locations at no fitness cost. Adding quorum signals to the medium also
84 amplifies *rhlA* gene expression in liquid culture, particularly when the cells are in early
85 stationary phase (Boyle et al. 2015).

86 The regulation of *rhlAB* expression integrates nutrient and quorum signal information and
87 depends on at least three diffusible molecules: a growth-limiting nutrient, and the hierarchical
88 quorum sensing structure involving the quorum signal molecules 3-oxo-C12-HSL and C4-HSL
89 (Latifi et al. 1996; Pearson et al. 1997; Ochsner and Reiser 1995; Ochsner et al. 1994; Wagner et
90 al. 2003; Medina et al. 2003). According to the literature, all three diffusive inputs, the two auto-
91 inducers as well as any small molecule growth-limiting nutrient, act on similar length/time
92 scales. In addition, the ratio of the diffusion coefficients and decay rates for these molecules in
93 bacterial growth media (Cornforth et al. 2014) indicate that the quorum signals could achieve
94 high enough levels to reach and influence biomass that is multiple millimeters away. Still, the
95 diffusible species may compete in their control of gene expression: growth nutrients such as
96 nitrogen and iron should downregulate *rhlAB* whereas quorum sensing signals should upregulate

97 *rhlAB*. The regulation of *rhlAB* in a spatially structured system may be quite complex and
98 sensitive to environmental fluctuation.

99 Considering the initial seeding of a swarming assay, at the center of an agar plate, we
100 hypothesized that the nutrient environment would deplete in the center of the swarm first and
101 then proceed outward, standard to population motility theory, with the region of active growth
102 localized to the edge of the swarming tendril at the interface between the population and growth
103 limiting resources (Deforet et al. 2019). We expected quorum signals to follow the reverse
104 pattern, building first in the center of the swarm with lowest levels at the swarming tendril tips.
105 Given liquid culture literature, this lead to a hypothesis where rhamnolipids are largely being
106 produced at the center of a swarm, where quorum signals are high and growth rate is low, with
107 minimal production at the tendril tips where quorum signals are low and growth rate is high.

108 Here we analyze image timeseries of *P. aeruginosa* swarms fluorescently labeled for
109 biomass production and P*rhlAB* activity (Supplementary Figures 1-3, and 5). We find that,
110 contrary to our hypotheses, the edges of swarming tendrils emerge as the regions of highest
111 cooperative gene expression. To interrogate the role of the diffusive inputs on *rhlAB* expression
112 in describing this phenotype, we used immotile colonies seeded as in the classic Colony Forming
113 Unit (CFU) assay to investigate how the interactions between colonies affect rhamnolipid
114 production. Using these data, we fit an ecological kernel through regularized regression
115 motivated by reaction-diffusion principles showing that both growth rate information and colony
116 neighborhood configuration are critical to explain the complex gene expression we observed.
117 Finally, we show that quorum signals, known to facilitate cellular communication over
118 micrometer distances (Darch et al. 2018; Connell et al. 2010; Connell et al. 2014), are capable of
119 centimeter-scale communication between *P. aeruginosa* colonies. Further, while perturbation by

120 quorum signals in liquid culture never showed significant alteration to *rhlAB* expression, the
121 same perturbation in the spatially structured system surprisingly revealed an over-expression
122 phenotype that was nonetheless cost-less in both bacterial colonies and motile swarms. Taken
123 together, these data show that there are new regimes of bacterial gene expression yet to be
124 unlocked in spatially-structured systems. Our findings reveal new scales of bacterial
125 communication and new dimension to the evolutionary robustness of bacterial cooperation.

126 Results

127 Expression of *rhlAB* peaks at the edge of swarming colonies

128 Competition for nutrient and quorum sensing are two types of cell-cell interactions
129 mediated by diffusible processes that affect *rhlAB* expression. Their competing influences make
130 the dynamics of *rhlAB* expression in motile swarms difficult to predict. We constructed a
131 fluorescent imager inside an incubator to track cell growth and *rhlAB* expression directly in
132 colonies on Petri dishes (Supplemental Figure 1), using a *P. aeruginosa* PA14 strain with a dual-
133 label construct harboring PBad-DsRed(EC2) (Pfleger et al. 2005) driven by L-arabinose which
134 was included in the plate media (Newman and Fuqua 1999) and P*rhlAB* -GFP (van Ditmarsch
135 and Xavier 2011; Boyle et al. 2015). The constitutive expression of DsRed provided an
136 indication of the local density of bacteria (Supplemental Figure 2), and the dynamical expression
137 of GFP reported on the expression of *rhlAB*. The data was corrected for uneven lighting of the
138 samples (Supplemental Figures 1, 3, see Methods).

139 Using this imaging device we investigated swarming (Figure 1a). Counter to our
140 expectations, that *rhlAB* expression peaked at the tip of each swarming tendril rather than at the
141 center of the swarming colony. To confirm this observation, we quantified expression along the

142 length of three tendrils from four independent swarming colonies throughout the time course of
143 the swarm (Figure 1b). The *rhlAB* expression increased with the distance from the swarm center
144 in all cases. This dynamic coincides with an unexpected growth phenotype in the swarming
145 tendrils (as reported by the red signal): The biomass across the entire tendril showed an
146 exponential growth rate (Figure 1c inset), which was particularly surprising as the average
147 spreading velocity of the tendril is linear at 3.2mm/h with a standard deviation of 0.8 mm/h.
148 To characterize how an exponential growth rate could emerge in a tendril advancing
149 linearly, we analyzed three regions within the swarming tendril: the center of the swarm, a fixed-
150 sized region in the middle of the tendril, and the edge. Pixels were isolated and used to calculate
151 the average behavior in each region (Figure 1c). These swarms formed tendrils after an average
152 of 7.25 hours of growth with a standard deviation of 21 minutes. Surprisingly, the biomass level
153 at the center of a swarm continued to grow exponentially long after tendrils had formed and
154 started to move away from the initial seeding location. Similarly, the mid-tendril region also
155 maintained an exponential growth phase both regions showing doubling times of approximately
156 two hours.
157 The edge of a swarming colony is where fresh nutrients abound and where growth is
158 presumed to be fastest. However, part of the biomass produced is left behind as the edge of the
159 tendril as moves forward in a traveling wave (Deforet et al. 2019), and that biomass seeds the
160 mid tendril. Our observation that the mid tendril maintains exponential growth indicates that the
161 edge moves forward before the nutrients below are fully consumed.
162 As we do not control for flux of biomass between tendril regions, the growth rate
163 measured represents a combination of growth and migration into and out of each region.
164 However, as the general flow of the biomass is away from the swarm center, to first

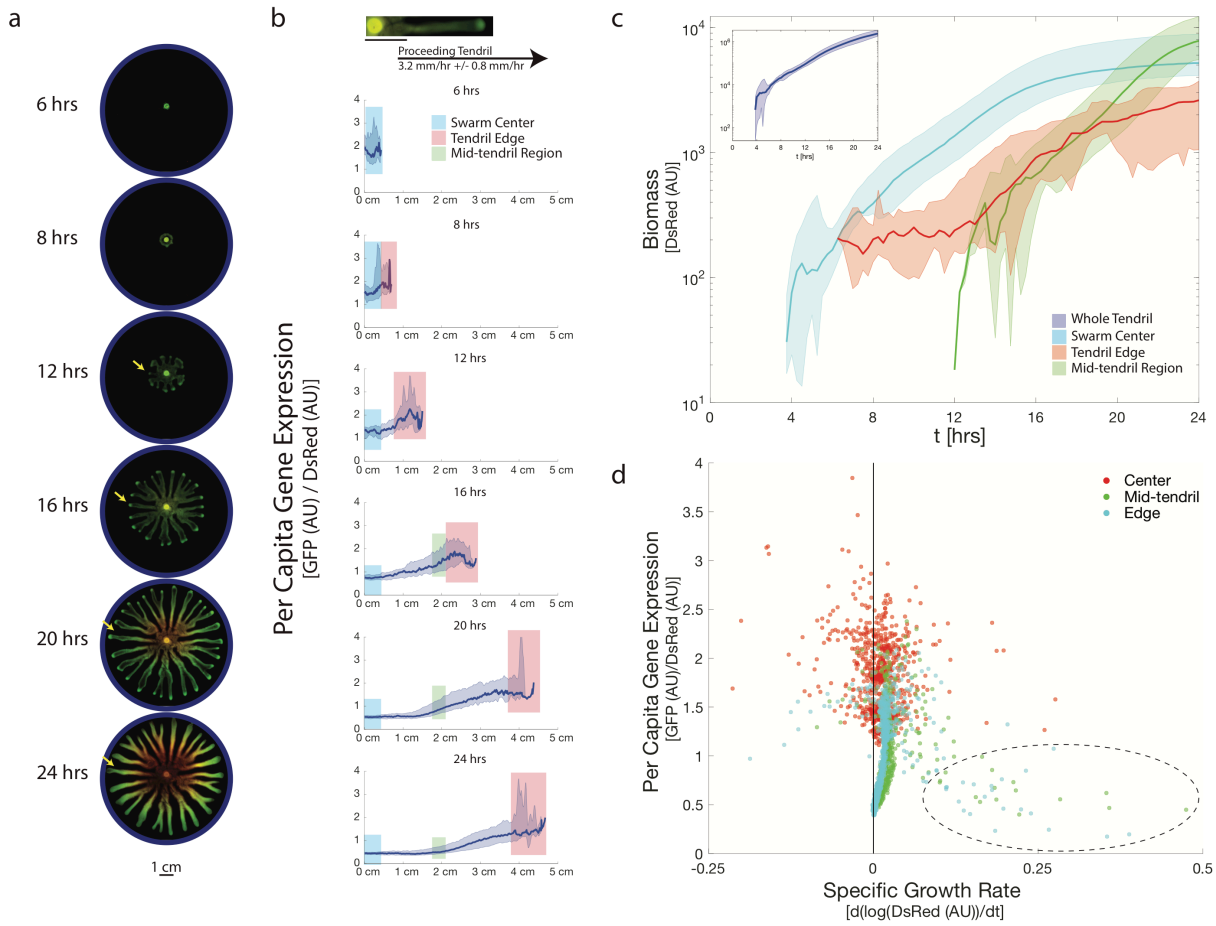

Figure 1: Swarming tendrils move with linear velocity, grow exponentially and show spatially segregated gene expression for rhamnolipid production

a. Swarms were imaged in 5-minute intervals across a 24-hour period. Cells are fluorescently labeled for biomass (constitutive marker for biomass PBad-DsRed (EC2) induced by L-arabinose in the plate media) (red channel) and activity of the *rhlAB* operon (through the promoter fusion P*rhlAB*-GFP) (green channel). Images of selected timepoints were background corrected (see Methods) and are contrasted to the maximum intensity found in all images in the timeseries. **b.** Per capita gene expression is tracked by the ratio of GFP (P*rhlAB*-GFP) to DsRed (used as a biomass marker) per pixel. Data across three tendrils in each of four independent swarms were combined for analysis. We observe that the highest investment is surprisingly found at the edge of the swarm. Median gene expression data is highlighted and full range of the data is shaded. Max and min data was smoothed again for visualization. All tendrils were aligned to start at the same location for analysis though tendrils reach different final lengths. **c. Inset:** Total biomass identified along the length of isolated tendrils with time. We observe that the whole tendril appears to sustain an exponential rate of growth throughout the timeseries. **Main Panel:** Biomass with time for three sections of the swarm: Center (blue), mid-tendril (cyan) and swarm edge (red) for the same tendrils as in **b**. Data normalized for size of region isolated. Median data plotted in bold, area shaded is full range of the data. Max and min data was smoothed for visualization. Note that the mid-tendril maintains an exponential growth rate after

182 the edge of the tendril has passed. We also find that the edge of a swarming colony appears to sustain a rate of
183 increase in localized biomass similar to the mid-tendril. **d.** Per capita gene expression plotted against the growth rate
184 of each region of the swarm. Growth rate determined as the derivative of the log of the red data. We find the swarm
185 center and mid-tendril regions have lower per capita gene expression at high growth rate and higher at low growth
186 rate, consistent with previous reports (Boyle et al. 2015; Xavier et al. 2011). We find that at our lowest observed
187 growth rates, gene expression drops, consistent with (Boyle et al. 2015). Per capita gene expression at the swarm
188 edge is noticeably higher than the mid tendril or swarm center, though the variation is not clearly explained by the
189 growth rate of biomass localized to the swarm tip.

190 approximation the flux into the center or mid tendril can be neglected. The growth rate calculated
191 for the edge of a tendril likely underestimates the cellular growth rate in that region because there
192 is unlikely to be flux into the tendril tip, and only flux out of it (the biomass left behind as the
193 edge moves away from the seeding location).

194 To investigate whether any region of the swarm behaved similarly to expected
195 metabolically prudent dynamics, we analyzed each region's per capita gene expression with
196 respect to the corresponding growth rate (Figure 1d). In the center and mid-tendril of the swarm,
197 we observe that high growth rates correlate with lower levels of per capita gene expression
198 (Figure 1d dashed circle). This indicates that the cells may indeed be titrating gene expression in
199 accordance with local nutrient availability as in liquid culture (Boyle et al. 2015). However, at
200 the edge we find no correlation between *rhlAB* expression and measured growth rate. As we are
201 likely underestimating the true growth rate of the biomass at the edge, this result was puzzling
202 given current knowledge of the inherent gene expression control. Overall, locally the swarm
203 tendril behind the swarm tip seemed to be behaving in accordance with known metabolic
204 prudence, however, globally the high per captia gene expression localization to the tendril tip
205 remained unexplained.

206

207 Experiments on hard agar recapitulate spatial-temporal dynamics of *rhlAB* 208 expression without the complication of movement

209 Studying the dynamics of growth and *rhlAB* expression in swarming colonies is
210 complicated by the difficulty of separating growth rates from motility flux in the regions
211 examined above. Swarming requires an agar concentration of 0.5%, and increasing the
212 concentration to 1.5% is enough to prevent swarming (Xavier et al. 2011). In hard agar, a strip of

213 immotile PA14 (Supplementary Figure 4a) revealed the same pattern of *rhlAB* expression in this
214 immotile model of a tendril with *rhlAB* expression peaking at the edges (Supplemental Figure
215 4c). However, the immotile tendril was unable to sustain an exponential growth rate
216 (Supplemental Figure 4b), indicating that this gene expression phenotype may be able to be
217 explained by the diffusive inputs to this system.

218 To probe the role of solute diffusion on *rhlAB* expression we continued to use hard agar
219 experiments to prevent motility (Figure 2a). Using extreme dilution of bacterial inocula (Figure
220 2b) we seeded colony forming units (CFUs) and tracked the development of those colonies from
221 single cells to mature colonies. We computed growth and *rhlAB* expression for each individual
222 colony (Supplemental Figure 3, 5). Using a range of experiments, we varied the number of
223 colonies and their local distribution in each Petri dish to produce thousands of growth and *rhlAB*
224 expression curves and capture a wide diversity of gene expression behaviors.

225 Our data showed that colonies located in regions of higher local density grew to smaller
226 colony sizes at 48 hours compared to colonies in less dense regions of the same plate. This is
227 expected from the effects of nutrient depletion from local crowding (Figure 2d) and can be
228 captured by the variation in the amount of biomass within a 4.5mm radius neighborhood of each
229 colony. The *rhlAB* expression curves, however, revealed an unexpected diversity of dynamics
230 that showed a very complex dependency on local neighborhood. We found that while the peak
231 per capita gene expression in a focal colony correlated with the amount of biomass within a
232 4.5mm radius neighborhood, but the correlation between a colony's neighborhood its per capita
233 gene expression varies in both amplitude and sign with time (Figure 2e).

234 One way to characterize these data was to ascertain how the variation in each colony's
235 per capita gene expression could be explained by the current state of the system. We

236 hypothesized that if the *rhlAB* expression level of each colony depended only on the focal colony
237 itself then each colony's *rhlAB* expression signal would correlate with its corresponding biomass
238 signal. Conversely, if colony-colony interaction played a key role then *rhlAB* expression would
239 not correlate with the colony's biomass level. To test this, we took the *rhlAB* gene expression at
240 each timepoint and asked if the variation could be explained by the size of each colony at the
241 same timepoint. We found that early in our timeseries, *rhlAB* expression does correlate well with
242 red levels (Figure 2f – Dark Blue Curve). However, later in the timeseries, there is a drop in the
243 *rhlAB* expression variation that can be explained by the biomass signal. To investigate the
244 remaining variation we calculated the per capita gene expression by calculating the ratio of the
245 total green fluorescence to the total red fluorescence for each colony. We find that as the
246 correlation between the GFP and DsRed signal declines the variation in the ratio that can be
247 explained by the biomass in a focal colony's 4.5mm neighborhood starts to increase (Figure 2f –
248 Cyan curve). This analysis indicated that colony-colony interactions may indeed alter the *rhlAB*
249 expression of each individual colony.
250

251 Growth state alignment and regularized regression quantifies the interaction 252 between neighboring colonies

253 Next we sought to detail the function by which each radius of a focal colony's
254 neighborhood influenced its *rhlAB* expression. We collected timeseries from colonies started
255 from single cells, generating thousands of independent experiments in high throughput. Each
256 colony came above detection by our pipeline at a slightly different time, even among colonies on
257 the same plate. This made it difficult to understand how two colonies with similar growth
258

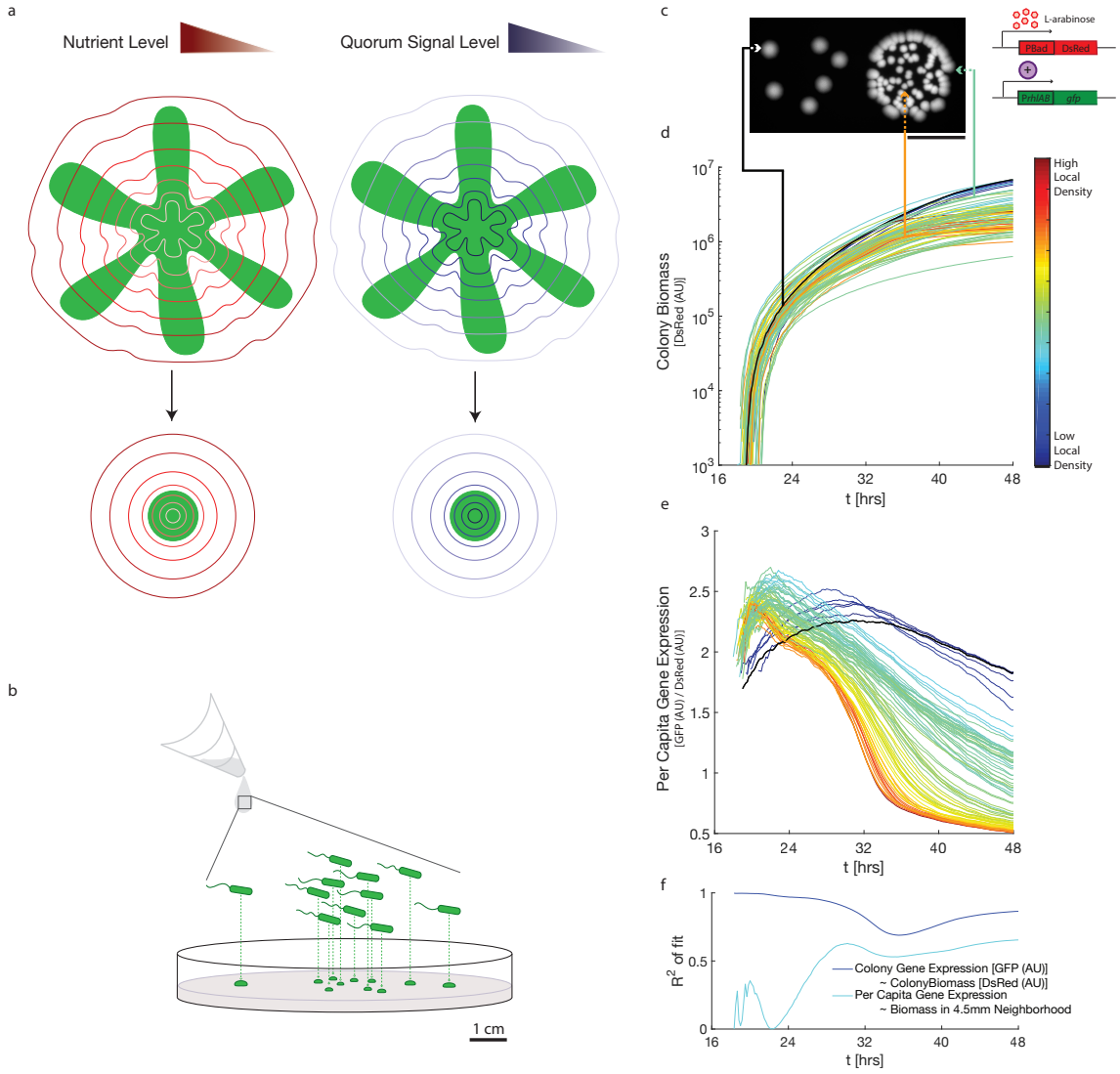

Figure 2: Colony Forming Units as a model system for emergent growth and cooperation patterning

a. Growth and cooperation dynamics that emerge from nutrient and quorum signal diffusion can be studied in hard agar diffusive systems. [Top] Cartoon depicting hypothesized nutrient and quorum signal fields in developed swarms. [Bottom] Cartoon depicting the simplified fields predicted of developing colonies. **b.** Method of generation for of Colony Forming Unit (CFU) plates. A washed and dilute culture is placed and left to dry on the plate. Colonies that emerge were seeded from individual single cells. (See Methods) **c.** CFU image at 48 hours. Data characterizes colony biomass as indicated by intensity of the shown DsRed image. Scale bar 1 cm. Colonies indicated are highlighted in D and E. Schematic describes fluorescent labeling used. (See Figure 4a for more information on the *rhlAB* regulation pathway.) **d.** Analysis of image timeseries (see Methods and Supplementary Figure 1-3 and 5) generates a growth curve for each colony. Colony growth trajectories are colored by the number of colonies within a 4.5mm radius of the focal colony. Variation in colony growth curves correlates, as expected, with spatial configuration. Colonies highlighted demonstrate the variation observed in the dataset. **e.** Colony per capita

gene expression of *rhlAB* operon calculated as in Figure 1. Coloration of the expression data as in D reveals that in this dataset, many neighbors in a 4.5mm radius correlates with an earlier peak in per capita gene expression. **f.** Explanation of variation observed in colony per capita gene expression. Data at each timepoint is independently fitted to the indicated model and goodness of fit shown. We observe that much of the variation in colony gene expression varies with colony biomass (Dark blue curve). However, this correlation decays with time. At later timepoints, variation in colony per capita gene expression, can be explained by the amount of non-self biomass in a 4.5mm neighborhood around the focal colony. This indicates that the colonies may be able to influence the gene expression of one another.

280 trajectories (Figure 3b inset) could have such different per capita gene expression patterns
281 (Figure 3b main panel). However, we noticed that the growth rate of each colony was predictive
282 of its per capita expression dynamics (Figure 3b main panel). At high growth rate, colonies had
283 low levels of per capita gene expression. Between a small range of low growth rate, the per
284 capita gene expression peaked. Below a threshold growth rate, gene expression turned off. Using
285 this information, we grouped colony data by growth rate. These similarities allowed us to
286 investigate how the neighborhood surrounding a colony could generate variation in per capita
287 gene expression.

288 To quantify the colony-colony interaction, we inferred a spatial interaction kernel directly
289 from our data. We computed the amount of biomass (using the red signal) in concentric
290 neighborhoods around each focal colony (Figure 3a). These neighborhoods were then used as
291 features to explain variation in *rhlAB* per capita expression. We grouped data across growth
292 curves and four independent experiments with similar configurations of colonies by growth rate
293 (Figure 3b) and we applied ridge regularization to fit three models, one for each growth rate bin
294 (Figure 3c). The results revealed a complex spatial-temporal pattern of activation and inhibition
295 that results from the different length-scales of the diffusional factors as the colonies developed.
296 However, we noticed the coefficients corresponding to the influence of each neighborhood on a
297 focal colony's behavior showed a pattern: The coefficients of a given neighborhood often shared
298 the same sign across all three regressions, but differed in amplitude (Figure 3c blue white and red
299 bar). This may indicate that in a given configuration, there is a fixed spatial interaction kernel
300 and the colony's growth rate is indicative of the colony's ability to respond to the information in
301 that kernel.

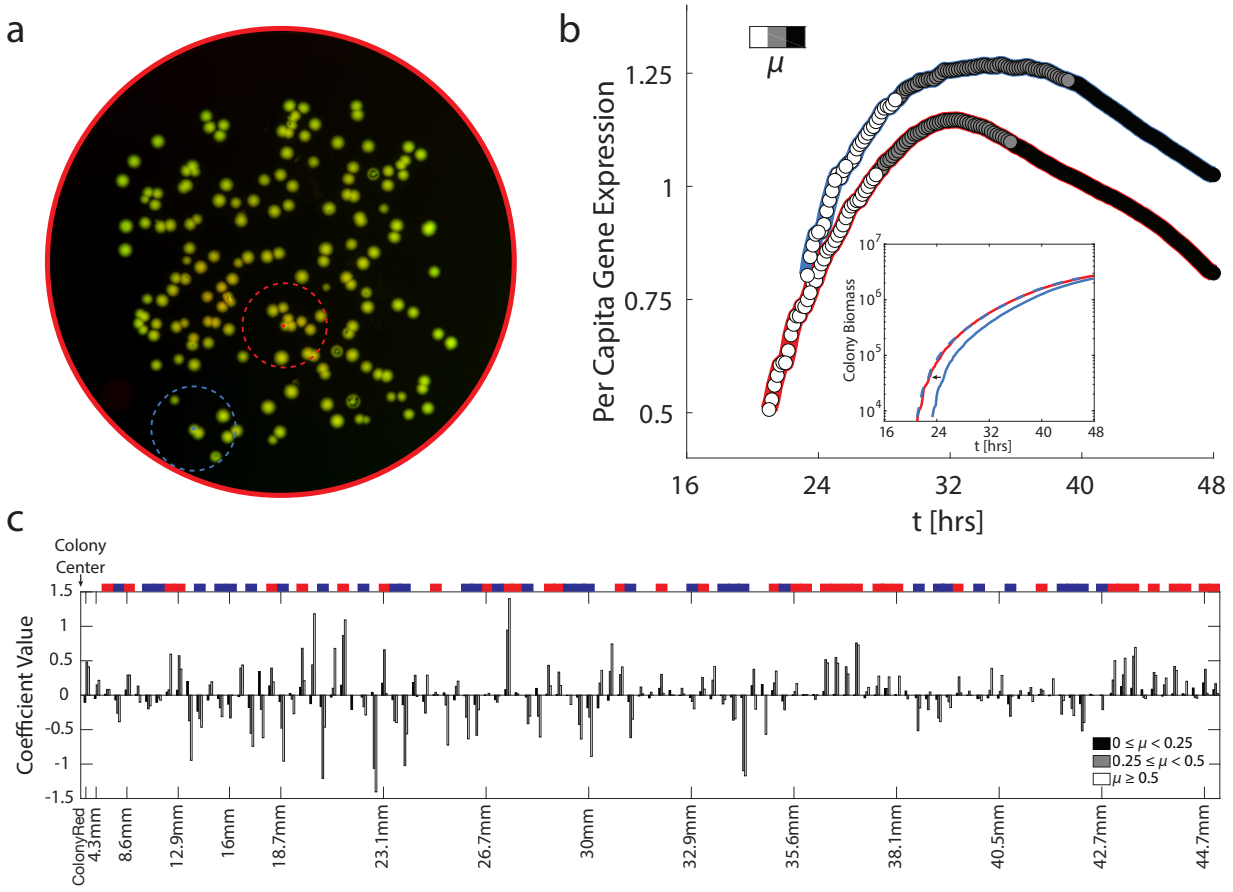

Figure 3: The spatial-temporal gene expression patterning from the integration of nutrient and quorum signal information can be described through a spatial kernel that changes with local density

a. Two colonies and respective example neighborhoods, indicated by blue and red dashed circles. **b.** Colonies with similar growth curves can show strong differences in gene expression dynamics but similarities appear when data is grouped by growth rate. [Inset] Two colonies (the ones indicated in **a**) have similar growth dynamics, as shown by the time shifted blue colony curve (dashed blue line). [Main Panel] Per capita gene expression patterns vary between the two colonies, however growth rate, μ, (high (white), medium (gray), low (black)) correlates with changes in gene expression dynamics. Periods of high growth rate correlate with increasing levels of gene expression, intermediate growth rates correlate with peak levels of gene expression, and low growth rate correlates with declining per capita gene expression. **c.** Ridge regularized results describing the kernel of interaction in each of the three growth rate bins. Data across four experiments with configurations like that shown in **a** are included. In general, the coefficient describing the influence of biomass in that neighborhood on a focal colony is either positive (red) or negative (blue) with the scale of the response varying with the growth rate of the focal colony. Coloration above the plot is used whenever all three growth rate bins show the same coefficient sign, inclusive of 0. R^2 values in Supplementary Table 1.

318 **Signal-negative mutants validate distance-dependent activation of *rhlAB***
319 **expression**

320 Next, we sought to confirm that one of the inputs responsible for the rich dynamics in
321 *rhlAB* expression was a response to quorum signals. To do this, we utilized a mutant unable to
322 produce the 3-oxo-C12-HSL and C4-HSL signals, PA14 Δ*lasI*Δ*rhlI* double-labeled in the same
323 way as the WT, as a quorum signal receiver (Figure 4a). To isolate the quorum signal response,
324 we focused on a colony's response to the C4-HSL molecule, the furthest downstream of the two
325 quorum signals. Tracking P_{rhlAB} activity showed whether that colony had sensed both quorum
326 signals. We added 1μM 3-oxo-C12-HSL to the plate media and placed 4μL of 5μM C4-HSL on
327 a filter paper on the center of a petri dish and we tracked the growth and *rhlAB* expression in
328 colonies started from single cells seeded around the filter paper (Figure 4b). The mutant colonies
329 showed maximal *rhlAB* per capita gene expression at the colony peak that was inversely
330 proportional to the colony's distance to the filter paper (Figure 4c, d), $R^2 = 0.37$. However, there
331 was a batch effect that corresponded with the number of colonies on the plate where plates with
332 fewer colonies (light blue data points) showed higher per capita gene expression overall than
333 colonies with a denser colony seeding (dark blue and black data points).

334

335 **Perturbation with quorum signals reveals a spatially-linked expression**
336 **pattern that scales with distance to the quorum signal source**

337 These experiments carried out with the signal negative mutant confirm that diffusible
338 quorum signals explain part of the spatial-temporal pattern of *rhlAB* expression. We did not
339 expect, however, that adding quorum signals to the media would influence the colony behavior

340 of WT bacteria. Previous work done in liquid culture showed no change in total rhamnolipid
341 production in WT bacteria grown with quorum signals added to the media (Xavier et al. 2011).
342 Surprisingly, when quorum signals were added to the same plate media recipe, WT colonies
343 seeded far from each other expressed more *rhlAB* during periods of higher growth rate, even
344 when compared to other wild type (WT) colonies grown in similar configurations without added
345 quorum signals (Figure 4e).

346 To understand the discrepancy between the liquid culture versus spatially-structured
347 colonies, we looked to see if these expression dynamics replicated in the signal mutant. We
348 found that colonies close to the filter paper expressed *rhlAB* more at high growth rate than those
349 far from the filter paper source (Figure 4g). This behavior could be quantified by fitting colony
350 expression at high growth rate with a decaying exponential function (Figure 4f,g). In doing so we
351 uncovered a threshold-like detection response (Figure 4g). Colonies less than 2.5-3cm from the
352 quorum signal source show a similar induction pattern with little variation in per capita gene
353 expression at high growth rate, just as we observed in our WT colonies with supplemented
354 quorum signals. Farther than 2.5cm away, the exponential decay coefficients vary linearly with
355 colony distance to the source ($R^2 = 0.60$) and have a very low peak per capita gene expression.
356

357 Swarming is robust to cheating despite *rhlAB* overexpression by extrinsic
358 quorum signals

359 To test whether this alteration in gene expression carried a cost to cell growth, we
360 measured colony fitness in three independent ways. First, we looked for a change in the
361 distribution of growth rates of the colonies in the first time interval after detection. A lower

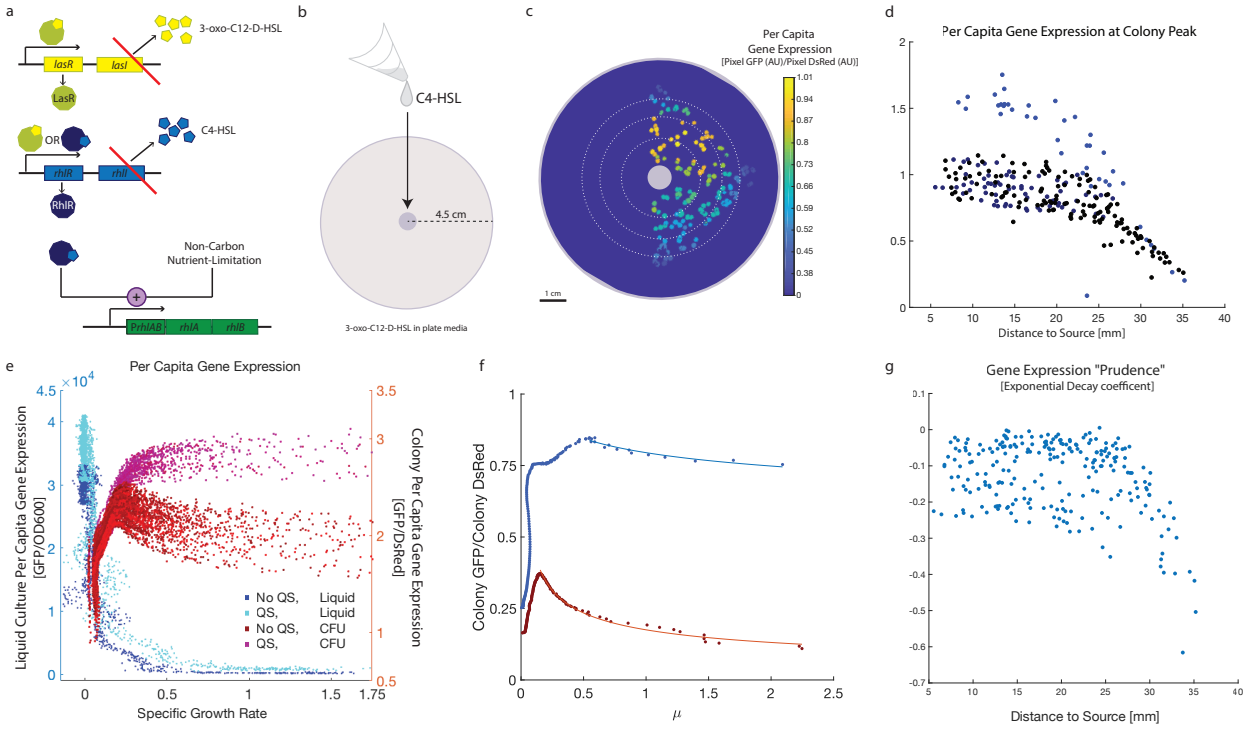

Figure 4: Perturbation with quorum signals reveals a spatially-linked expression pattern that scales with distance to the quorum signal source

a. The native molecular circuit determining *rhlA* expression. The molecular circuit and alterations (red lines) describes a signal mute quorum signal mutant that is unable to produce the two autoinducer molecules required for *rhlA* production. **b.** Experimental design to demonstrate the centimeter length scale of quorum signal response. The upstream quorum signal (3-oxo-C12-HSL) is added directly to the plate media and the downstream signal, C4-HSL, is loaded on a filter paper in the center of the plate. Colonies have been seeded around the filter paper and will respond if the colony observes both quorum signals. **c.** Signal mute colonies respond to diffusible quorum signals. Colony borders indicative of colony area after 24 hours of growth. Coloration indicates the maximum per capita gene expression achieved throughout the time-course at the colony peak. **d.** Per capita gene expression at colony peak correlates with the distance of the colony to the center of the filter paper. Data from three independent biological replicates with 40 (blue), 69 (dark blue) and 139 (black) colonies on the plates respectively. $R^2 = 0.3744$. **e.** Liquid and spatially structured expression patterns with respect to measured growth rate. Liquid culture per capita *rhlA* gene expression measured as GFP/OD600 (Xavier et al. 2011) when grown in liquid culture with (Cyan) and without (Blue) exogenous quorum signals. There is no clear difference in the per capita gene expression (Blue Axis) with quorum signal perturbation in liquid. However, immotile colonies grown without quorum signals (red) and with quorum signals in the plate media (magenta) show a clear difference in per capita gene expression (Orange Axis). Growth rate is calculated as the derivative of the log(DsRed) data with respect to time. Data for each experimental configuration includes three biological replicates. CFU data was taken from plates where colonies were grown at low numbers in low local density to minimize colony-colony interactions. Each datapoint represents a time interval in a liquid or immotile colony timeseries. **f.** Signal mute mutants closer to the quorum signal source show a higher

per capita gene expression regardless of growth rate. These dynamics are shown for two example colonies here. Colonies are indicated in **c**. To characterize the turn on pattern of this gene expression with respect to growth rate, we fit an exponential decay curve from high growth rate, to the growth rate with maximal per captia gene expression. The orange colony at 35.06 mm from the quorum signal source shows a strong correlation between per capita gene expression and growth rate. By contrast, the blue colony at 7.17 mm from the quorum signal source shows a response that is roughly independent of the growth rate and has a much smaller in magnitude exponential decay coefficient. **g.** Colony location relative to the quorum signal source (the filter paper) explains variation in temporal dynamics of per captia gene expression. Colony gene expression is characterized by the coefficient of the exponential decay fit of the data from maximal growth rate to maximal investment across the time course. This analysis reveals that colonies less than 2.5-3cm from the quorum signal source have low exponential decay coefficients indicating that the per capita expression remains close to the colony's maximum value even during periods of high growth. Exponential decay coefficients beyond 25mm from the source vary linearly with their distance to the source with $R^2 = 0.60$.

397 growth rate under quorum signal perturbation would have indicated a growth cost prior to
398 detection. We found no difference between these growth rate distributions in experiments with
399 and without quorum signal perturbation with colonies in similar configurations nor in plates with
400 an alternative configuration also perturbed with quorum signals (Figure 5a). Next, we looked for
401 a difference in the final colony size. If the colonies in the perturbation were smaller at the end of
402 the timeseries, a growth cost may have occurred in a less obvious way during the time interval of
403 colony observation. We found instead that the colonies that were grown with added quorum
404 signals were the same size as colonies grown without quorum signal when in a similar
405 configuration (Figure 5b). Finally, we looked for a transient cost, a temporal element to the
406 behavior that could indicate a comparatively different state of growth when comparing datasets
407 grown with and without quorum signals. We compared the distributions of the times when the
408 colonies, come above detection. Here, we saw indeed that colonies grown with quorum signals
409 can come above detection later than colonies grown without (Figure 5c). When quorum signal
410 mutants are subjected to quorum signals they can stay in lag phase longer (Boyle et al. 2015),
411 and this may be what occurred here for the for WT bacteria growing in media with added
412 quorum signals.

413 To see if this phenotype also played a role in the motile swarming model system, we
414 searched for an increase in *rhlAB* expression in the motile swarms. Indeed, we found that adding
415 both autoinducers to the media media accelerated the onset of swarming by ~30 minutes
416 compared to swarms without supplemented autoinducers (Figure 6a).

417 With the observations that quorum signal perturbation leads to increased per capita gene
418 expression in immotile colonies and earlier onset of tendril formation, we asked if this
419 perturbation could involve a fitness cost when the WT is in competition with an established

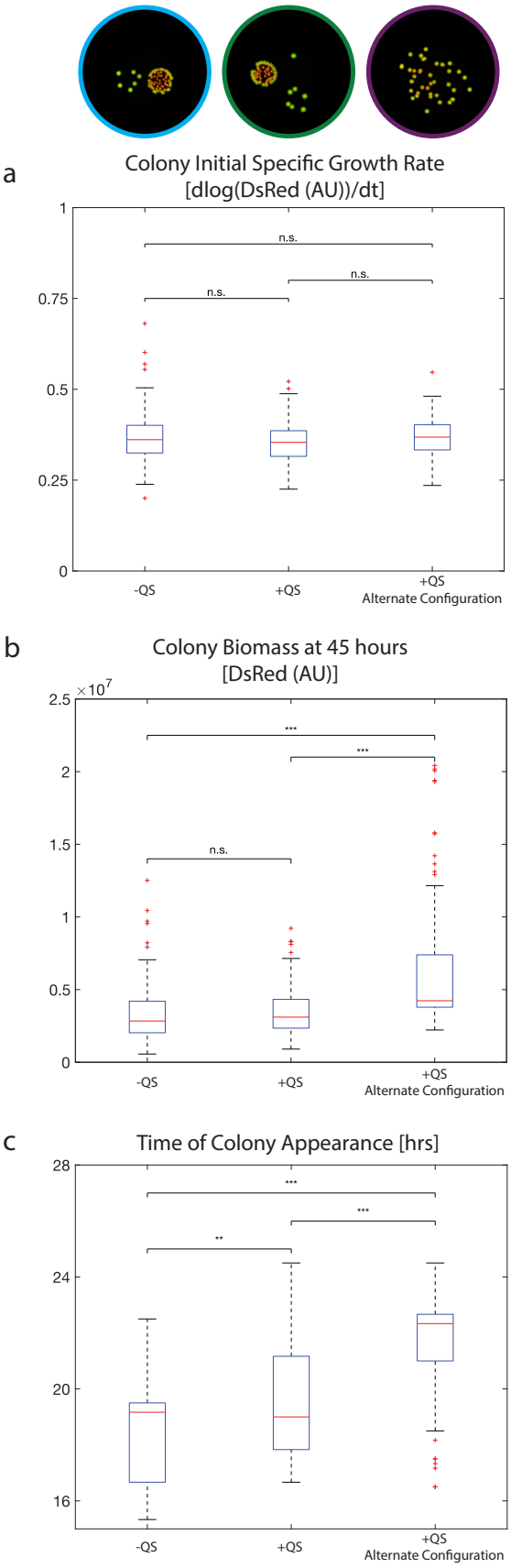

Figure 5: Quorum signal perturbation reveals no growth impact

a. Comparison of growth rate at the time of colony appearance with and without quorum signals in the media. Three biological replicates of three colony configurations were compared. Representative datasets pictured at the top. [Left configuration] colonies organized with high configuration variation. [Center configuration] colonies organized as in the left configuration, colonies perturbed with quorum signals in the media. [Right configuration] Colonies grown with low configuration variation, spread far apart on the plate. Media contains quorum signals at the same levels as the center configuration data. Colonies growth with or without quorum signals in the plate media show no difference in initial growth rate. Colonies grown at lower local density with quorum signals in plate media also show no difference in initial growth rate distribution. Colony identification algorithm was consistent across datasets [See Methods]. Significance measured by the Mann-Whitney test (See Supplemental Table 2). **b.** Comparison of final colony biomass at 45 hours with the same 9 datasets as in A. Colonies grown with quorum signals in the media were found to have a similar size distribution to colonies grown without quorum signals in a similar colony configuration by the Mann-Whitney test. Colonies grown farther apart grow to larger final size. Quorum signal perturbation does not lead to any apparent growth cost we observe at 45 hours. **c.** Comparison of time of colony appearance. Colonies grown without quorum signals are found to appear earlier than colonies grown with quorum signal. Significance measured by Mann-Whitney test.

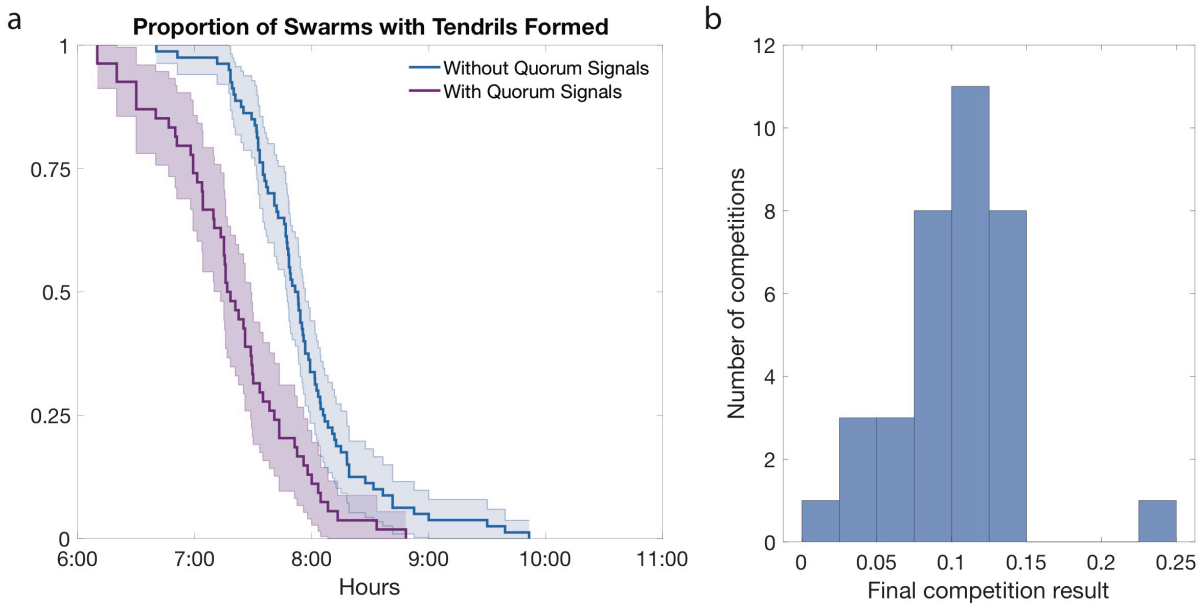

Figure 6: Quorum Signal perturbation reveals accelerated cooperative behavior but no competitive disadvantage in mixes with rhamnolipid-deficient free riders

a. Swarming start times with and without autoinducer in the plate media. No QS: 8 biological replicates with 80 total technical replicates. QS: 6 biological replicates with 54 total technical replicates. p-value <1e-8 by Kolmogorov-Smirnov test. **b.** WT PA14 was competed at a 1:1 ratio against the Δ*rhlA* strain with quorum signals in the plate media (see methods). After competition for 24 hours the plates were washed and the cells diluted and counted by CFU. The change in the proportion of the WT strain (Final ratio WT/(Total Cell Number) – Initial Ratio (0.5)) at the conclusion of the competition is shown. Initial frequencies were recorded and final ratios calculated with respect to these. Data includes three biological replicates with several technical replicates in each. See Supplementary Table 3 for initial ratios and final population sizes for each competition.

468 defector mutant (Xavier et al. 2011; de Vargas Roditi et al. 2013). Surprisingly, we saw no
469 competitive cost to the WT when quorum signals were added to the swarming plate media
470 (Figure 6b). Since there is no visible growth cost, we conclude that—despite our attempts to
471 perturb *rhlAB* expression—swarming cooperation remains robust to cheating.

472

473 # Discussion

474 Here, we used a combination of experimental and computational methods to advance our
475 knowledge of *rhlAB* expression in a spatially-structured environment. We developed a novel
476 high-throughput analysis, using fluorescence to track spatial-temporal bacterial growth and gene
477 expression. The data produced showed that the gene expression in motile swarming *P.*
478 *aeruginosa* colonies peaked at the tip of each tendril, a finding unexpected from our previous
479 understanding of *rhlAB* expression (Figure 1). This phenotype emerged regardless of cell
480 motility (Supplementary Figure 4). Further, we found that swarming tendrils, while expanding at
481 a linear velocity, were able to maintain an exponential growth rate. This exponential growth rate
482 is generated by a sustained growth rate throughout the tendril, not localized to the tendril edge as
483 expected. This may be an example of navigated range expansion, following recent observations
484 of growth dynamics in motile *E. coli* strains (Cremer et al, 2019).

485 To explore this unintuitive phenotype, non-motile colonies started from single cells
486 provided a valuable model to study the communication between bacterial aggregates via
487 diffusible compounds impacting gene expression and cooperative behavior. We found the
488 immotile colony an underappreciated model that produced massive amounts of data to
489 characterize growth and gene expression with spatial interaction (Figure 2). Even with classic

490 microbiology assays we believe new layers of regulation to bacterial behavior can be quantified,
491 perturbed and characterized that were not present in the equivalent liquid culture experiments.
492 Our analysis not only revealed that *P. aeruginosa* colonies can communicate across
493 centimeter scale distances (Figure 4), it showed that colony communication through the
494 integration of growth and quorum signal information is capable of generating complex regions of
495 both positive and negative interactions between colonies that further vary with the configuration
496 of the cell aggregates and scale with the colony's growth rate (Figure 3). The kernels of
497 interaction that we built from these data can be used to generate hypotheses of relevant length
498 and growth timescales that may provide insight into the robustness of social interaction and
499 cooperative phenotypes in natural bacterial communities.
500 Furthermore, the imaging infrastructure we have described allows for high throughput
501 iteration between the immotile and motile systems. The volume of the data we were able to
502 collect using immotile colonies allowed us to uncover a spatially-linked perturbability to
503 cooperative gene expression whereby the colonies are able to express *rhlAB* at levels previously
504 uncharacterized by liquid culture experiments (Figure 4). Surface-induced gene expression has
505 been seen before in biofilm polymer production and cell shape changes have been observed in
506 the transition from planktonic life to swarming (Davies and Geesey 1995; Sauer et al. 2002;
507 Kuchma and O'Toole 2000; Sauer and Camper 2001; McCarter and Silverman n.d.; Davies et al.
508 1993; Harshey and Matsuyama 1994). However, these studies focus on the presence of gene
509 expression in bacteria attached to surfaces or present in biofilms that wasn't present in liquid.
510 *rhlAB* expression occurs regardless of surface or liquid environment in *P. aeruginosa*. In this
511 study, we uncovered a new, spatially-linked perturbability to *rhlAB* expression, giving a social

512 degree of freedom to the control of this cooperative behavior that becomes possible when cells
513 are on a surface or moving in a swarm.
514 While our immotile colony data indicated there was no growth cost under social
515 perturbation (Figure 5), work in the motile swarms indicated that this increased gene expression
516 pattern played a role in the fully motile system (Figure 6a). This gives us a unique opportunity to
517 ask if this behavior could play a role in the competitive motile system (Figure 6). Finding no
518 competitive disadvantage to this increased expression pattern, we conclude this new regime of
519 gene expression falls under the metabolic prudence regulation structure. However, we note that
520 quorum signal perturbation likely has systemic effects and that the impact we observed on the
521 time to tendril formation in the swarms is likely dependent on more than rhamnolipid production
522 alone.
523 To crystalize how *rhlAB* expression changes with both growth rate and social
524 environment, we submit Figure 7 as a model for this system. Biomass (red) growth rate (black)
525 and per capita gene expression (green) are representations of data previously presented and
526 analyzed (Figure 1). The quorum signal curve (blue) is an approximation of the quorum signal
527 field assuming a constant production rate with growth rate. The key elements to the integration
528 of nutrient limitation and quorum signal concentration are as follows. When the cells are
529 growing with a high growth rate, cells are more susceptible to perturbation by quorum signal
530 (Figure 3c and Figure 4d). This means that when biomass is growing at a similar rate and with a
531 similar amount of biomass, as can be seen in comparing the center of a swarm before tendril
532 formation (Figure 7a) with the tip of the tendril at 12 hours (Figure 7b), the tip of the tendril,
533 exposed to a higher quorum signal concentration, will express more *rhlAB* per capita. This also
534 means that when exposed to the same quorum signal levels but experiencing a difference in
535

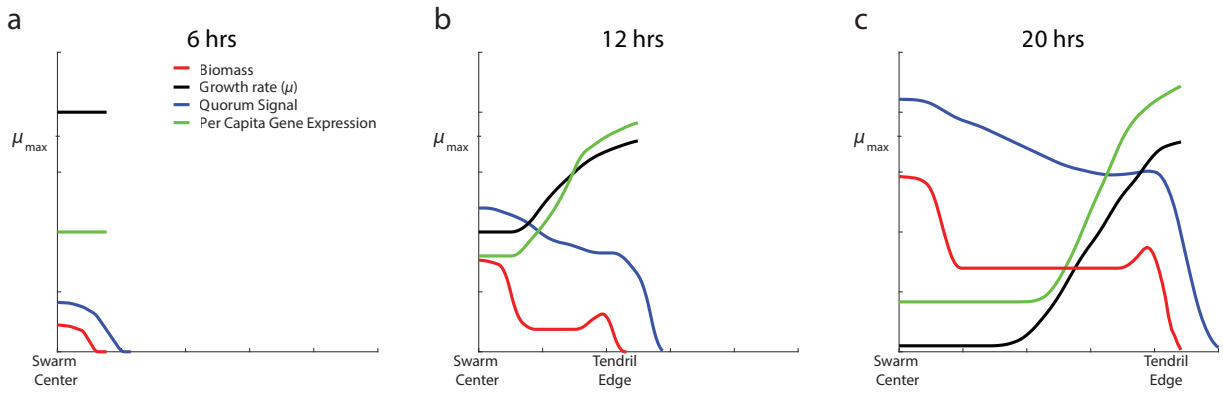

Figure 7: The combination of nutrient information and quorum signals allows for the emergence of directionality

Cartoon depicting three key timepoints in swarming tendril development. Cross sectional biomass density overlaid with distance dependent growth rate, quorum signal concentration and per capita *rhlAB* expression. **a**. At 6 hours, no tendrils have formed, biomass is largely localized at the original seeding location. Growth rates in the cells are high and quorum signals are less than maximal. Gene expression is uniform per unit of biomass throughout the population. **b**. At 12 hours, the tendril is moving at a constant velocity, growth is localized to the edge of the tendril and the biomass localizes at the tendril tip. Quorum signals continue to be produced in the center of the swarm, the rest of the tendril produces quorum signals proportional to the regions biomass level and growth rate. The gene expression that results is still moderate at the swarm center, but now highest at the tip of the tendril, correlating with the highest growth rate. **c**. At 20 hours, the tendril tip may be experiencing quorum signal levels similar to those of the center given a production rate proportional to the growth rate and diffusion of the signals. However, the comparatively high growth rate in this region allows a distinction between quorum signal levels accumulated over time (swarm center) and the resultant low gene expression, and quorum signal levels accumulated due to rapid growth and the corresponding high gene expression.

553 growth rate, cells growing at a slower rate will express less *rhlAB* per capita. This can be seen by
554 comparing the gene expression at the slow-growing swarm center at 12 hours (Figure 7b) with
555 the same quorum signal concentration experienced by the tip of the swarm tendril at 20 hours
556 (Figure 7c). Taken together, a metabolically prudent basis for gene expression with high
557 perturbability at high growth rate could explain the emergent directionality of *rhlAB* per captia
558 gene expression that we observe experimentally.

559 Bacteria exist in complex social and spatial environments, but very little is known
560 regarding cellular decision-making in these highly dynamic and spatially-driven environments.
561 The basis of our understanding of bacterial behavior comes from studying regulation
562 mechanisms thoroughly but in liquid culture. However, bacteria live mostly in spatially-
563 structured environments. Experimental models such as *P. aeruginosa* swarms and even immotile
564 colonies growing on hard agar allow us to study proximate molecular mechanisms and ultimate
565 evolutionary questions in spatially structured communities (Yan et al 2019). Spatially structured
566 environments are able to recapitulate a range of behavior in natural bacterial communities
567 unattainable by liquid culture experiments. By iterating experimental and computational data-
568 driven methods we demonstrate that the integration of quorum signal and nutrient limitation
569 information in the metabolically prudent regulation of *rhlAB* can still let the tip of a swarming
570 tendril emerge as a region of high cooperative gene expression. Further, we show that this gene
571 expression control is robust to cheating across a much wider range of conditions than previously
572 appreciated by liquid culture experiments. As many social behaviors take in diffusive inputs, this
573 result may be generalizable to a wide range of social or cooperative phenotypes with spatially-
574 linked gene regulation that can already be assayed with classic microbiology techniques.
575

576 # Materials and Methods

577 **Microbiological assays**

578 Plates were made with the recipe described in (Yan et al. 2019) with the addition of
579 1.8mL of L-arabinose at 40% weight/volume for a concentration of 1.5%. Water was subtracted
580 to compensate. Every plate has 20mL of agar media and was inspected visually to confirm a flat
581 surface. Swarms were prepared as described in (Yan et al. 2019). Liquid culture assays were
582 performed using casamino acid media prepared as in (Xavier et al. 2011). Data was acquired on a
583 benchtop TECAN plate reader. The data was analyzed using custom software in MATLAB
584 (Boyle et al. 2015).

585 All timeseries were imaged with prototype imaging setup, Canary (Supplemental Figure
586 1). Fluorescent LEDs were used to light the sample. Data was collected by Atik VS14
587 Fluorescent Camera through the Thorlabs filter wheel FW102C. Timeseries was collected
588 through a custom-built control system using the Arduino Uno R3. Immotile colony timeseries
589 were imaged every 10 minutes. Swarms were imaged every 5 minutes. Images taken in Canary
590 were subject to uneven lighting due to the placement of the fluorescence LEDs (Supplementary
591 Figure 1). To correct for this, multiple plates were imaged in Canary as well as on a flatbed
592 scanner. We called this scanner data our 'ground truth'. A correction was built from these images
593 that allowed us to take each image generated in Canary and alter it to the evenly lit environment
594 on the scanner. This correction was built manually by extracting features from the images. The
595 data was validated on rotational datasets taken in Canary (Supplementary Figure 3). The final
596 background correction is shown below. Parameters vary depending on the exact configuration of
597 Canary though the terms remain consistent. The correction was updated as the instrument
598 received upgrades and to control for variation in the L-arabinose batch used.

599

600 $$R_{Scanner} = a + bx + cy + dxy + eR_{Colony}(1 + fx + gy) + h(Distance\ To\ Plate\ Center)(1 + iR_{Colony})$$

601

602 Min and max biomass and gene expression data full range boundaries from swarming
603 tendrils (Figures 1bc) was smoothed once with a moving window of 5 for visualization.
604 Background corrected pixel data is smoothed once with a moving window of 5 along the time
605 axis before pixel data is extracted and grouped into colony components. Colony Red data is
606 smoothed once with a moving window of 5 before exponential growth rates of the colonies are
607 calculated.

608 Unless noted otherwise, swarms and colonies provided exogenous quorum signals were
609 perturbed with the concentration of quorum signals determined to be present after 24 hours of
610 swarming (Xavier et al. 2011).

611

612 **Analysis of immotile colonies**

613 Cells were grown overnight in Casamino acid media and passaged into fresh Casamino
614 acid media for 2-4 hours to reach exponential phase. These cells were then triple washed, diluted
615 and spotted onto the agar such that every colony arises from a single cell. Colonies were plated
616 with motility-preventing agar concentrations as in the classic Colony Forming Unit (CFU) assay
617 (Figure 6a,b). The cells were fluorescently labeled for both biomass generation and rhamnolipid
618 investment. Biomass was tracked using DsRed(DC2) (Pfleger et al. 2005) under the control of
619 the PBad promoter induced by L-arabinose in the plate media (Figure 6c, Figure 2) (Newman
620 and Fuqua 1999). Rhamnolipid investment was tracked through the previously validated P*rhlAB*
621 -GFP promoter fusion (van Ditmarsch and Xavier 2011; Boyle et al. 2015).

622 The image timeseries post-processing was done in MATLAB R2018a (Supplemental
623 Figures 3 and 5) and used to generate colony-centric growth, per captia gene expression
624 information and all spatial-temporal features used in the text.
625 To supplement the identification of colonies, we developed a method to separate colonies
626 that grow together and "merge" over the course of the timeseries so they could be tracked
627 independently. After the images were background corrected, the peaks of the colonies were
628 identified across a range of images and parameter values. The images used are between 20 and
629 30 hours, before the majority of colony merge events. The best parameters for peak identification
630 were selected and used in the downstream analysis.
631 Each complete image timeseries was used to create a mask with all pixels that will
632 eventually contain biomass. Once identified, each pixel was tracked throughout the timeseries.
633 To localize pixels to their cognate colony, the previously identified peaks, the mask and the
634 biomass distribution in the final timepoint were used with the watershed algorithm to identify the
635 boundaries of colony objects.
636 L2 (Ridge) regularization was performed with a 4-fold cross validation (Figure 3c).
637
638 **Analysis of swarming colonies**
639 To determine the speed of a moving tendril, the location of the edge every 15 minutes
640 between 12 and 20 hours was calculated and the data was smoothed with a moving window of
641 1.25 hours. Swarms were imaged in a prototype imager equipped with a fish eye lens allowing
642 for the acquisition of brightfield data for up to twelve swarming plates at a time. The timeseries
643 were analyzed in ImageJ to identify the time of tendril formation. As the fish eye lens spreads the
644 image pixels to cover a much larger region, the signal to noise ratio was managed carefully when

collecting these data. Tendril formation times for each plate were calculated at three different zoom levels and averaged. To avoid bias, the data for each plate was collected by at least two independent researchers before averaging.

Acknowledgements

The authors acknowledge Ned Wingreen, Chris Myers, Kyu Rhee, Dan Heller, Jinyuan Yan, Bradford P. Taylor and Chen Liao for helpful discussions and manuscript comments. This work was funded by National Science Foundation (www.nsf.gov) award MCB- 1517002/NSF 13-520 to JBX and a National Science Foundation Graduate Research Fellowship GRFP DGE-1257284 2012 to HM.

Bibliography

Boyle, K.E., Monaco, H., van Ditmarsch, D., Deforet, M. and Xavier, J.B. 2015. Integration of metabolic and quorum sensing signals governing the decision to cooperate in a bacterial social trait. *PLoS Computational Biology* 11(5), p. e1004279.

Caiazza, N.C., Shanks, R.M.Q. and O'Toole, G.A. 2005. Rhamnolipids modulate swarming motility patterns of *Pseudomonas aeruginosa. Journal of Bacteriology* 187(21), pp. 7351–7361.

Connell, J.L., Kim, J., Shear, J.B., Bard, A.J. and Whiteley, M. 2014. Real-time monitoring of quorum sensing in 3D-printed bacterial aggregates using scanning electrochemical microscopy. *Proceedings of the National Academy of Sciences of the United States of America* 111(51), pp. 18255–18260.

Connell, J.L., Wessel, A.K., Parsek, M.R., Ellington, A.D., Whiteley, M. and Shear, J.B. 2010. Probing prokaryotic social behaviors with bacterial "lobster traps". *mBio* 1(4).

Cornforth, D.M., Popat, R., McNally, L., et al. 2014. Combinatorial quorum sensing allows bacteria to resolve their social and physical environment. *Proceedings of the National Academy of Sciences of the United States of America* 111(11), pp. 4280–4284.

Costerton, J.W., Stewart, P.S. and Greenberg, E.P. 1999. Bacterial biofilms: a common cause of persistent infections. *Science* 284(5418), pp. 1318–1322.

Darch, S.E., Simoska, O., Fitzpatrick, M., et al. 2018. Spatial determinants of quorum signaling in a *Pseudomonas aeruginosa* infection model. *Proceedings of the National Academy of Sciences of the United States of America* 115(18), pp. 4779–4784.

Davies, D.G., Chakrabarty, A.M. and Geesey, G.G. 1993. Exopolysaccharide production in biofilms: substratum activation of alginate gene expression by Pseudomonas aeruginosa. *Applied and Environmental Microbiology* 59(4), pp. 1181–1186.

Davies, D.G. and Geesey, G.G. 1995. Regulation of the alginate biosynthesis gene algC in Pseudomonas aeruginosa during biofilm development in continuous culture. *Applied and Environmental Microbiology* 61(3), pp. 860–867.

Deforet, M., Carmona-Fontaine, C., Korolev, K.S. and Xavier, J.B. 2019. Evolution at the edge of expanding populations. *The American Naturalist* 194(3), pp. 291–305.

Deng, P., de Vargas Roditi, L., van Ditmarsch, D. and Xavier, J.B. 2014. The ecological basis of morphogenesis: branching patterns in swarming colonies of bacteria. *New journal of physics* 16, pp. 015006–015006.

Déziel, E., Lépine, F., Milot, S. and Villemur, R. 2003. *rhlA* is required for the production of a novel biosurfactant promoting swarming motility in *Pseudomonas aeruginosa*: 3-(3-hydroxyalkanoyloxy)alkanoic acids (HAAs), the precursors of rhamnolipids. *Microbiology* 149(Pt 8), pp. 2005–2013.

van Ditmarsch, D. and Xavier, J.B. 2011. High-resolution time series of Pseudomonas aeruginosa gene expression and rhamnolipid secretion through growth curve synchronization. *BMC Microbiology* 11, p. 140.

Drescher, K., Nadell, C.D., Stone, H.A., Wingreen, N.S. and Bassler, B.L. 2014. Solutions to the public goods dilemma in bacterial biofilms. *Current Biology* 24(1), pp. 50–55.

Fu, X., Kato, S., Long, J., et al. 2018. Spatial self-organization resolves conflicts between individuality and collective migration. *Nature Communications* 9(1), p. 2177.

Granato, E.T., Meiller-Legrand, T.A. and Foster, K.R. 2019. The evolution and ecology of

700 bacterial warfare. *Current Biology* 29(11), pp. R521–R537.
701 Griffin, A.S., West, S.A. and Buckling, A. 2004. Cooperation and competition in pathogenic
702 bacteria. *Nature* 430(7003), pp. 1024–1027.
703 Harshey, R.M. and Matsuyama, T. 1994. Dimorphic transition in Escherichia coli and
704 Salmonella typhimurium: surface-induced differentiation into hyperflagellate swarmer cells.
705 *Proceedings of the National Academy of Sciences of the United States of America* 91(18), pp.
706 8631–8635.
707 Kim, W., Racimo, F., Schluter, J., Levy, S.B. and Foster, K.R. 2014. Importance of positioning
708 for microbial evolution. *Proceedings of the National Academy of Sciences of the United States of*
709 *America* 111(16), pp. E1639-47.
710 Kuchma, S.L. and O'Toole, G.A. 2000. Surface-induced and biofilm-induced changes in gene
711 expression. *Current Opinion in Biotechnology* 11(5), pp. 429–433.
712 Latifi, A., Foglino, M., Tanaka, K., Williams, P. and Lazdunski, A. 1996. A hierarchical
713 quorum-sensing cascade in Pseudomonas aeruginosa links the transcriptional activators LasR
714 and RhlR (VsmR) to expression of the stationary-phase sigma factor RpoS. *Molecular*
715 *Microbiology* 21(6), pp. 1137–1146.
716 Lee, H.H., Molla, M.N., Cantor, C.R. and Collins, J.J. 2010. Bacterial charity work leads to
717 population-wide resistance. *Nature* 467(7311), pp. 82–85.
718 Lejeune, O., Tlidi, M. and Lefever, R. 2004. Vegetation spots and stripes: Dissipative structures
719 in arid landscapes. *International journal of quantum chemistry* 98(2), pp. 261–271.
720 McCarter and Silverman MicroReview Surface-induced swarmer cell differentiation of Vibrio
721 parahaemoiyticus.
722 Medina, G., Juárez, K., Valderrama, B. and Soberón-Chávez, G. 2003. Mechanism of
723 Pseudomonas aeruginosa RhlR transcriptional regulation of the rhlAB promoter. *Journal of*
724 *Bacteriology* 185(20), pp. 5976–5983.
725 Mellbye, B. and Schuster, M. 2014. Physiological framework for the regulation of quorum
726 sensing-dependent public goods in Pseudomonas aeruginosa. *Journal of Bacteriology* 196(6), pp.
727 1155–1164.
728 Nadell, C.D., Bucci, V., Drescher, K., Levin, S.A., Bassler, B.L. and Xavier, J.B. 2013. Cutting
729 through the complexity of cell collectives. *Proceedings. Biological Sciences / the Royal Society*
730 280(1755), p. 20122770.
731 Nadell, C.D., Foster, K.R. and Xavier, J.B. 2010. Emergence of spatial structure in cell groups
732 and the evolution of cooperation. *PLoS Computational Biology* 6(3), p. e1000716.
733 Newman, J.R. and Fuqua, C. 1999. Broad-host-range expression vectors that carry the L-
734 arabinose-inducible Escherichia coli araBAD promoter and the araC regulator. *Gene* 227(2), pp.
735 197–203.
736 Ochsner, U.A., Koch, A.K., Fiechter, A. and Reiser, J. 1994. Isolation and characterization of a
737 regulatory gene affecting rhamnolipid biosurfactant synthesis in Pseudomonas aeruginosa.
738 *Journal of Bacteriology* 176(7), pp. 2044–2054.
739 Ochsner, U.A. and Reiser, J. 1995. Autoinducer-mediated regulation of rhamnolipid
740 biosurfactant synthesis in Pseudomonas aeruginosa. *Proceedings of the National Academy of*
741 *Sciences of the United States of America* 92(14), pp. 6424–6428.
742 Pearson, J.P., Pesci, E.C. and Iglewski, B.H. 1997. Roles of Pseudomonas aeruginosa las and rhl
743 quorum-sensing systems in control of elastase and rhamnolipid biosynthesis genes. *Journal of*
744 *Bacteriology* 179(18), pp. 5756–5767.
745 Pfleger, B.F., Fawzi, N.J. and Keasling, J.D. 2005. Optimization of DsRed production in

Escherichia coli: effect of ribosome binding site sequestration on translation efficiency. *Biotechnology and Bioengineering* 92(5), pp. 553–558.
Rietkerk, M., Boerlijst, M.C., van Langevelde, F., et al. 2002. Self-organization of vegetation in arid ecosystems. *The American Naturalist* 160(4), pp. 524–530.
Rietkerk, M., Dekker, S.C., de Ruiter, P.C. and van de Koppel, J. 2004. Self-organized patchiness and catastrophic shifts in ecosystems. *Science* 305(5692), pp. 1926–1929.
Rutherford, S.T. and Bassler, B.L. 2012. Bacterial quorum sensing: its role in virulence and possibilities for its control. *Cold Spring Harbor perspectives in medicine* 2(11).
Sauer, K. and Camper, A.K. 2001. Characterization of phenotypic changes in *Pseudomonas putida* in response to surface-associated growth. *Journal of Bacteriology* 183(22), pp. 6579–6589.
Sauer, K., Camper, A.K., Ehrlich, G.D., Costerton, J.W. and Davies, D.G. 2002. *Pseudomonas aeruginosa* displays multiple phenotypes during development as a biofilm. *Journal of Bacteriology* 184(4), pp. 1140–1154.
Singh, P.K., Schaefer, A.L., Parsek, M.R., Moninger, T.O., Welsh, M.J. and Greenberg, E.P. 2000. Quorum-sensing signals indicate that cystic fibrosis lungs are infected with bacterial biofilms. *Nature* 407(6805), pp. 762–764.
Smith, P. and Schuster, M. 2019. Public goods and cheating in microbes. *Current Biology* 29(11), pp. R442–R447.
de Vargas Roditi, L., Boyle, K.E. and Xavier, J.B. 2013. Multilevel selection analysis of a microbial social trait. *Molecular Systems Biology* 9, p. 684.
Velicer, G.J. and Vos, M. 2009. Sociobiology of the myxobacteria. *Annual Review of Microbiology* 63, pp. 599–623.
Wagner, V.E., Bushnell, D., Passador, L., Brooks, A.I. and Iglewski, B.H. 2003. Microarray analysis of Pseudomonas aeruginosa quorum-sensing regulons: effects of growth phase and environment. *Journal of Bacteriology* 185(7), pp. 2080–2095.
Xavier, J.B., Kim, W. and Foster, K.R. 2011. A molecular mechanism that stabilizes cooperative secretions in *Pseudomonas aeruginosa*. *Molecular Microbiology* 79(1), pp. 166–179.
Yan, J., Monaco, H. and Xavier, J.B. 2019. The ultimate guide to bacterial swarming: an experimental model to study the evolution of cooperative behavior. *Annual Review of Microbiology* 73, pp. 293–312.
Zhu, K. and Rock, C.O. 2008. RhlA converts beta-hydroxyacyl-acyl carrier protein intermediates in fatty acid synthesis to the beta-hydroxydecanoyl-beta-hydroxydecanoate component of rhamnolipids in *Pseudomonas aeruginosa. Journal of Bacteriology* 190(9), pp. 3147–3154.